IOP Publishing Physics in Medicine and Biology
Phys. Med. Biol. (XXXX) XXXXXX https://doi.org/XXXX/XXXX

EPR-Imaging of magnetic field effects on radiation dose distributions around air cavities

Sebastian Höfel[1,2], Michael K. Fix[3], Edmond Sterpin[4,5], Felix Zwicker[2], Malte Drescher[1]

[1] Department of Chemistry, Konstanz Research School Chemical Biology, University of Konstanz, Germany
[2] Klinik für Strahlentherapie/Radiologische Gemeinschaftspraxis, Gesundheitsverbund Landkreis Konstanz, Konstanz, Germany
[3] Division of Medical Radiation Physics and Department of Radiation Oncology, Inselspital, Bern University Hospital and University of Bern, Switzerland
[4] KU Leuven, Department of Oncology, Laboratory of Experimental Radiotherapy, Leuven, Belgium
[5] Université catholique de Louvain, Center of Molecular Imaging, Radiotherapy and Oncology, Brussels, Belgium

E-mail: sebastian.hoefel@uni-konstanz.de

Abstract

New hybrid radiotherapy treatment systems combining a MRI-scanner with a source of ionizing radiation are beeing introduced in the clinic. The necessary strong magnetic fields of MRI may considerably affect radiation dose distributions, especially at tissue-air interfaces due to the electron return effect (ERE).
The purpose of this work was to examine the feasibility of Electron Paramagnetic Resonance Imaging (EPRI) to measure magnetic field induced perturbations of dose distributions around air-cavities.
Air-filled fused quartz tubes with an inner diameter of 3 or 4 mm and with a wall thickness of 0.5 mm served as EPR probe material. The tubes were placed inside a PMMA phantom and irradiated by a 6 MV photon beam to doses of up to 600 Gy. The irradiations were performed in the presence or absence of a transverse, homogeneous magnetic field providing a magnetic field strength of approximately 1.0 Tesla. For this purpose, an in-house permanent magnet was used. The spatial distribution of radiation induced, unpaired electron spins in the quartz tube was subsequently detected by applying spin-echo detected EPRI. A 2D Imaging setup was used such that the spin density (SD) was integrated along the tube axis. A SD–dose calibration was determined and then applied to convert the reconstructed images of spin density to dose distributions.
The final EPRI results were compared with Monte Carlo (MC) radiation transport simulations based on the well-established GEANT4 toolkit.
Expressed in polar coordinates, the circular dose distributions detected by means of EPRI are quantitatively in good agreement (passrate > 93% for a 3%/10° gamma criterion) with the results that were obtained from the MC simulations. By comparing the presence with the absence of a 1 T magnetic field considerable dose enhancements (up to +28%) and reductions (down to -35%) within the quartz tubes were observed.
The results demonstrate the feasibility of spin-echo detected EPRI to measure magnetic field induced perturbations of dose distributions around small, cylindrical air cavities (diameter 3 - 4 mm). With regard to EPRI, fused quartz serves as a suitable probe material for measuring spatially highly resolved (below 100 µm) radiation dose distributions, yet high doses (600 Gy) are needed to obtain a sufficient signal-to-noise ratio within a measuring time of 24 hours.

Keywords: EPR imaging, dosimetry, radiotherapy, MR-Linac, irradiated quartz

1. Introduction

Modern radiotherapy treatment techniques aim to apply highly conformal radiation dose distributions, i.e. delivering high doses to the tumor cells while sparing surrounding healthy tissue. This approach requires accurate target volume localization and patient positioning prior to each treatment session as well as monitoring of anatomical changes to adapt the treatment if necessary. These requirements may be met by image guided radiotherapy (IGRT).

In recent years, magnetic resonance imaging (MRI) has been proposed to serve as imaging modality for IGRT. New hybrid treatment machines combining a source of high energy (MeV) photons with a MRI scanner have been developed [1,2,3,4] and are currently introduced in the clinic [5,6] as MR guided radiotherapy (MRgRT) devices. Compared to X-ray imaging systems MRI provides superior soft tissue contrast, adds no additional radiation dose to the patient and allows image acquisition in arbitrarily oriented planes. However, MRI implies strong, permanent, homogeneous external magnetic fields (0.35 T [1], 0.6 T [3], 1.0 T [4], 1.5 T [2]) during irradiation. Usually the orientation of the magnetic field lines is either parallel (longitudinal) [3,4] or perpendicular (transverse) [1,2,3] in relation to the treatment beam. In both setups, the Lorentz force affects the dose distribution by deflecting the trajectory of released electrons that exhibit velocity components perpendicular to the magnetic field lines [7]. Especially for transverse setups considerable changes in dose distribution may occur – particularly at tissue-air interfaces due to the so called electron return effect (ERE) [8,9]. Recently, Rubinstein et al. [10] showed the clinical relevance of the ERE. The authors provided evidence for an increase of radiation induced lung damage in mice that were irradiated in the presence of a transverse 1.5 Tesla magnetic field. Thus, magnetic field induced perturbations of dose distributions need to be thoroughly investigated when introducing MRgRT in the clinic.

Commercial dose calculation algorithms were extended to take the influence of magnetic fields into account [11]. However, experimental investigation and validation of magnetic field induced perturbations of dose distributions is challenging – particularly for doses at the vicinity of an air-boundary.

In the past 60 years Electron Paramagnetic Resonance (EPR) spectroscopy has been widely used to investigate the production, structure and reaction mechanisms of ionizing radiation induced free radicals in various substances [12]. EPR-Imaging (EPRI) is a sensitive method to visualize spatial distributions of unpaired electron spins by utilizing magnetic field gradients for spatial encoding [13].

In this work, X-Band spin-echo detected EPRI is performed to determine radiation dose distributions in irradiated fused quartz samples. Fused quartz forms very stable radicals upon irradiation [14,15]. The permanently remaining spin distribution of unpaired electron spins is subsequently detectable by EPRI. The work focuses on the measurement of magnetic field induced perturbations of radiation dose distributions around small, cylindrical air cavities (inner diameter of 3 or 4 mm). The experimental results are compared to Monte Carlo radiation transport simulations using the well-established Geant4 [16] toolkit.

2. Methods

2.1 Magnet construction

An in-house permanent magnet was used to provide a strong, homogeneous magnetic field of approximately 1.0 T during irradiation. It consists of two NdFeB permanent block magnets (10 cm x 3 cm x 10 cm) with magnetisation grade N52 (Fa. dogeo GmbH, Waldlaubersheim, Germany) that were mounted on an iron yoke according to Figure 1a.

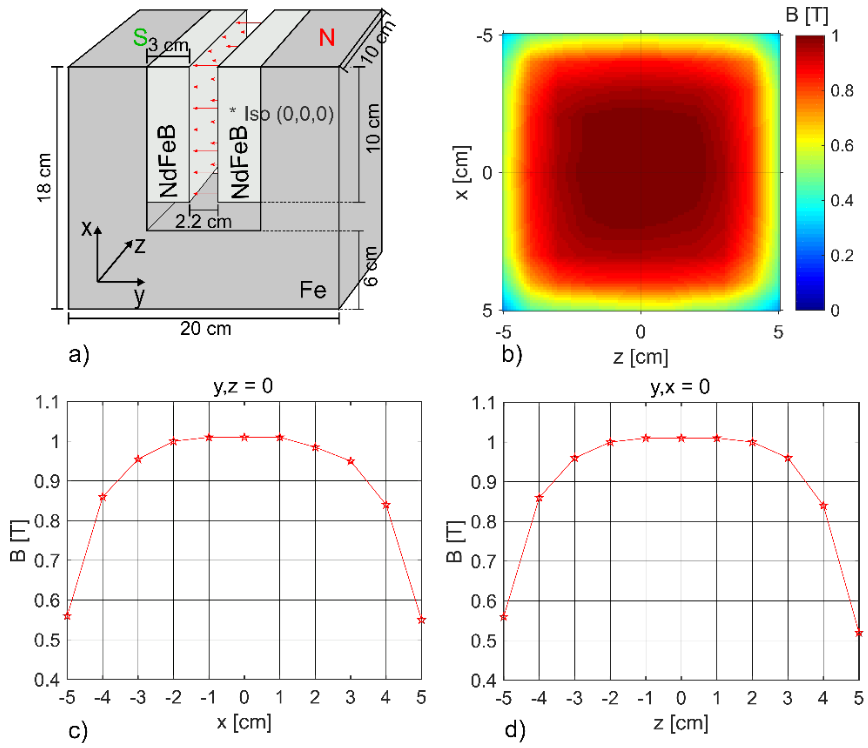

Figure 1: Permanent magnet construction and measurement results of the magnetic flux density distribution inside the air-gap. Physical dimensions of the magnet construction and definition of the 'magnet coordinate system' (a). The origin is defined as the centre of the air-gap. The magnetic field lines inside the air-gap run along the –y-direction. Interpolated magnetic field map in the central plane (x,0,z) (b). Linearly interpolated profiles in x-(c) and z-(d)- direction through the origin. The red asterisks reflect the points of measurement.

The magnetic flux density was measured inside the central plane (y,0,z) of the air-gap using a teslameter in combination with a hall-sensor (TETelectronics, Schönberg, Germany. Model 3103A and Model 688, respectively). The measurement results are depicted in Figure 1b-d.

The magnetic field map and profiles in Figure 1 clearly show a magnetic flux density ranging from 0.98 T at the edges to maximal 1.01 T within the central part (5 cm x 5 cm) of the (x,0,z) plane.

2.2 Samples and sample holders

As quartz samples pieces of ER221/TUB3 and ER221/TUB4 EPR sample tubes (Bruker BioSpin, Billerica, MA, USA) consisting of high quality clear fused quartz with a density of 2.2 g/cm³ (see Figure 2a) were used. TUB3 exhibits an inner diameter (I.D.) of 3 mm and an outer diameter (O.D.) of 4 mm. Whereas TUB4 has an I.D. of 4 mm and an O.D. of 5 mm. The tubes were cut in pieces of 8 mm length. For irradiation the samples were placed inside a dedicated composite PMMA phantom (Figure 2b). It consists of two outer PMMA plates (5 cm x 0.5 cm x 5 cm) and an inner PMMA plate (5 cm x 1 cm x 5 cm). The latter provided a central hole with either 5 mm or 4 mm diameter matching the O.D. of TUB4 and TUB3 samples, respectively.
For the EPRI measurements, the irradiated sample tubes were placed inside Teflon rods with an O.D. of 1 cm providing centred holes with corresponding diameters (Figure 2c).

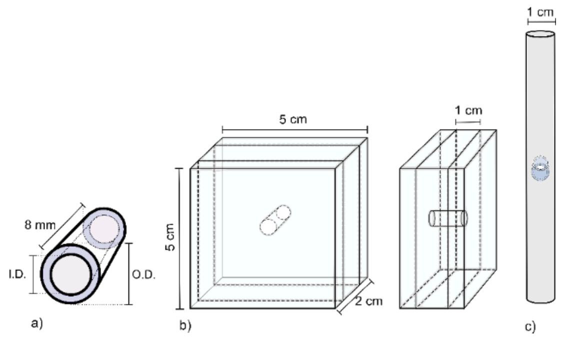

Figure 2: Definition of the inner and outer diameter (I.D. and O.D.) of the quartz tubes (a). PMMA phantom used for irradiation (b) and sample holder for EPRI experiment (c). Both provided a central hole of diameter 5 mm or 4 mm (depending on the O.D. of the quartz tube).

2.3 Sample Irradiation

All irradiations were performed using the flattening filter free 6 MV photon beam of a Tomotherapy® Hi-Art® (Accuray, Sunnyvale, CA, USA) treatment machine. A static vertical beam with a fixed field size of 9.1 cm x 2.5 cm (defined at a source-surface distance (SSD) of 85 cm) was selected by opening only the central 14 leaves of the binary multileaf collimator (MLC).
The quartz samples were placed inside the corresponding composite PMMA phantom (Figure 2b). The interior of the tubes was left air-filled. The PMMA phantom was then positioned centrally inside the air-gap between the NdFeB permanent magnets. The magnet construction containing the PMMA phantom was put on top of a water slab phantom and aligned with the treatment beam such that the quartz tube was located on the beam's central axis. The beam facing surface of the PMMA phantom had a distance of 62.5 cm from the radiation source (Figure 3). This setup minimized primary radiation through the magnet and still ensured that the PMMA phantom was completely covered by the beam. Note that the axis definition of the 'irradiation coordinate system' in Figure 3 matches the 'magnet coordinate system' (Figure 1a).

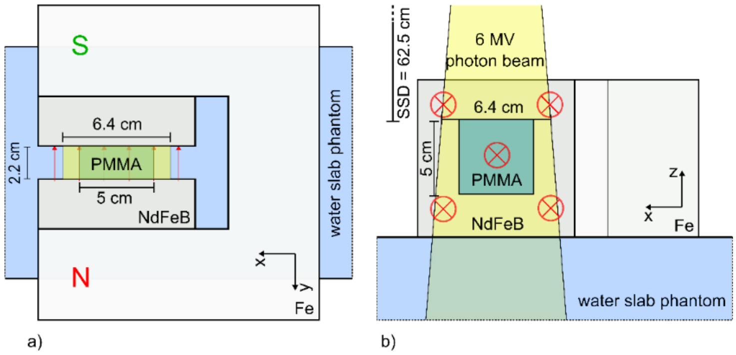

Figure 3: Irradiation setup and definition of the 'irradiation coordinate system'. Beam's eye view (a) and transversal section (b) of the setup used for irradiations in the presence of an external magnetic field.

Three different quartz samples were irradiated. Two (TUB3, TUB4) quartz tubes were irradiated in the presence of the magnetic field provided by the permanent magnet. An additional TUB4 sample was irradiated in no external magnetic field by using a non-magnetic dummy iron yoke (not shown) that had the same dimensions as the magnet but provided no magnetic field. All three samples were irradiated for 45 minutes to doses of 600 Gy.

2.4 EPRI Experiments

In this work pulsed EPR experiments were conducted at room temperature on a ELEXSYS E580 X-band EPR spectrometer (Bruker BioSpin, Billerica, MA, USA) operating in pulsed mode. In this mode sequences of short (ns-µs), high power microwave pulses are applied to the sample and spin-echo intensities are detected. The EPR absorption spectrum is detected by echo detected field sweeps (EDFS), i.e. recording spin-echo intensities while the magnetic field strength B_0 is swept.
EDFS measurements can be used in combination with magnetic field gradients to perform EPRI experiments. For this purpose, the E580 spectrometer was additionally equipped with a Bruker E 540 GCX2 gradient coil system. The coils provide magnetic field gradient strengths of up to 200 G/cm in z- and y- direction of the 'imaging coordinate system' depicted in Figure 4a. According to this coordinate system the B_0 field lines are parallel to the z-axis. By using both gradient coils simultaneously, the gradient of the magnetic field strength B_0 can be turned into any direction lying in the y-z-plane.
For echo detection the Bruker ER 4108 TMHS imaging resonator was overcoupled. This resonator is a flat cylindrical cavity resonant in the TM_{110} mode. The measured resonator y-profile is shown in Figure 4b. In the central 5 mm of the resonator the profile shows a plateau region, i.e. it varies by only 2.5 %. In z-direction the resonator profile is nearly flat (0-mode).

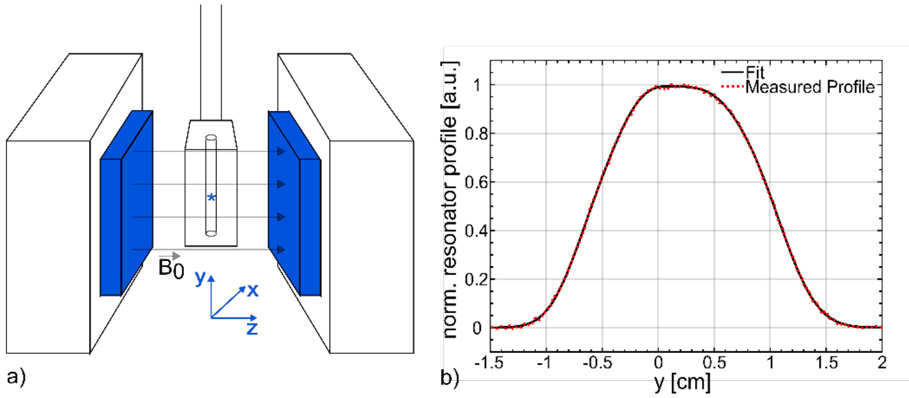

Figure 4: Schematic sketch of the imaging setup and definition of the 'imaging coordinate system' (a). The origin of the coordinate system is indicated by the asterisk. The gradient coil system (blue) is installed between the pole shoes of the electromagnet and the resonator. Measured and fitted echo intensity profile of the ER 4108 TMHS resonator (b) reflecting the distribution of the square root of the microwave power along the y-direction.

EPRI experiments were performed within three days after irradiation. The samples were inserted into the appropriate Teflon rod (Figure 2c) and positioned such that the center of the tubes was located at the center of the plateau of the resonator profile (Figure 4b). The direction of the quartz tube axis was aligned in parallel to the x-axis of the 'imaging coordinate system'.
A Hahn-echo sequence (π/2- π –echo) was applied to the sample. The EPR spectral width of irradiated quartz amounts in total to approximately 5 G. The spectrum exhibits a sharp feature of approximately 1 G width at the high-field edge of the spectrum. To minimize spectral line-shape distortions the excitation bandwidth was kept small by setting the π-pulse length to 1200 ns. The long phase memory time (T_M≈50 µs) allowed a respectively long time delay of 2 µs between the pulses. The spin-echo intensity was recorded by integrating the transient echo signal. Due to the long longitudinal electron spin relaxation time (T_1≈ 210 µs) the EDFS were acquired with a shot repetition time (SRT) of 2000 µs. A static gradient strength of 150 G/cm was applied and 140 projections (EDFS) were acquired by turning the gradient incrementally by 180 °/140 in the y-z-plane. The EPRI measurements ran for 22 – 24 h.
After each imaging experiment an EDFS was recorded with the same settings but with the magnetic field gradient turned off.

2.5 Image reconstruction

When applying magnetic field gradients to a sample the spatial information of spin density distribution is transformed to spectral information. In case that the spectral shape is constant throughout the sample, the EPR spectrum acquired under a certain gradient angle represents a convolution of the radon transform of the spin density under this angle with the spectral line shape [17].

No relevant variations in the spectral shape were observed among the quartz samples studied in this work. Therefore, it was assumed that the spectral line shape is constant throughout the irradiated sample and is equivalent to the integral spectrum given by the integral EDFS recorded subsequently after each imaging experiment. This is justified by the fact that the sampling resolution was reduced to approximately 10 points/Gauss for the imaging experiments and high spectral frequencies (> 0.5 1/G) were filtered out during deconvolution.

Each projection of the resulting sinogram was normalized to its integral intensity to compensate fluctuations in resonator sensitivity during the measurement. Afterwards the projections were deconvolved with the corresponding EDFS spectrum using the regularized filter algorithm of the MATLAB® (MathWorks, Nattick, MA, USA) function deconvreg. Since the EPR absorption spectrum of fused quartz features a steep signal fall off within approximately 1 G on the high-field edge of the spectrum one can expect a maximum imaging resolution of appoximately 53 µm when a gradient strength of 150 G/cm is applied. The pixel dimensions for the reconstruction matrix was set to comparable values (40 µm (TUB3) and 50 µm (TUB4)). These settings fitted well to the frequency filtering performed during deconvolution.

Following deconvolution, the 2D spatial spin distribution was reconstructed using the simultaneous iterative reconstruction technique (SIRT) [17]. For every reconstruction, 100 iterations and a (256 x 256) pixels matrix were applied. After reconstruction, the spin density distribution was corrected for the resonator profiles in z- and y-direction.

For the imaging setup of this work, the reconstructed images resulting from the EPRI experiments depict the radiation induced relative spin density (SD) distribution in the y-z-plane. Thus, each pixel of the reconstructed image represents the integral spin density along the tube axis.

2.6 SD-dose dependency

To convert the reconstructed image of relative spin density distribution to a dose distribution the SD-dose dependency was investigated. For this calibration purpose, four additional TUB3 quartz tubes were irradiated by the Tomotherapy beam to doses of 704, 515, 304 and 141 Gy, respectively. The irradiations were performed inside a water slab phantom and no magnetic field was applied.

Relative spin densities were derived from three consecutive 1D-EPRI experiments on composite samples (double stack) where the high dose sample (704Gy) was always measured in combination with one of the lower dose samples. Hence, the high dose sample served as intensity reference for each experiment. The measurement results showing a steplike profile were deconvolved with the absorption spectrum (EDFS). The mean step intensities were then calculated and corrected for the corresponding sample masses. Relative step intensities were then plotted against the corresponding relative dose values. By applying a polynomial fit to this data a SD-dose calibration curve was obtained.

2.7 Monte Carlo Simulation

MC Simulations were performed with version 10.3 of the Geant4 [16] toolkit. The low-energy electromagnetic models for electron and photon interactions were activated by selecting G4EmPenelopePhysics as physics list. The lower energy threshold limit for production of secondary particles was lowered to 100 eV and the range cut for the production of secondary electrons and photons was set to 0.05 mm according to the minimum dimension of the voxels of the scoring volume (see below).
The simulation geometry was defined corresponding to the irradiation setup shown in Figure 3. For the NdFeB magnets an alloy material according to the elemental composition with a density of 7.6 g/cm³ was created.
In the simulations considering a magnetic field during irradiation a global uniform magnetic field of 1 Tesla along the -y direction was assumed. The step size limitations (*dRoverRange* = 0.003, *finalRange* = 1nm), the tracking parameters in magnetic fields (*DeltaChord* = 1 µm, *MinimumEpsilonStep* = 5e-5, *MaximumEpsilonStep* = 5e-5, *DeltaIntersection* = 1 µm, *DeltaOneStep* = 1 µm) as well as the multiple scattering parameters (*RangeFactor* = 0.01, *GeomFactor* = 2.5 and *skin = 2*) were set according to Lee et al. [18]. A time efficient 4th order Runge-Kutte-Nystrom stepper (G4NystromRK4) was activated to integrate the equation of motion of a particle inside a homogeneous magnetic field. To define the Tomotherapy radiation beam, a validated phase-space file [19] was implemented. The position of the dose scoring volume with dimensions (8 mm x 8 mm x 8 mm) was defined such that the center of the scoring volume coincided with the quartz tube axis. The volume was divided in 160 bins along the z- and x-direction.
The relative standard errors for the mean dose values inside the quartz tubes resulting from 20 independent runs were below 2%.

3. **Results**

3.1 SD-Dose dependency

1D-EPRI experiments were performed on dedicated 'calibration samples' (section 2.6) to determine a calibration function that converts relative spin density values to relative dose values. These measurements were conducted on day 1 and day 18 after irradiation to check the reproducibility of this approach. The post processed (section 2.6) results for both days are shown in Figure 5.
The relative spin densities and relative dose values are normalized to an irradiation dose of 600 Gy. The relative standard errors for the derived relative spin densities were below 1.5 %.
The results of both days are identical within this uncertainty. Thus it can be concluded that signal fading within 18 days post irradiation does not affect the SD-dose calibration.
For the investigated dose range, the relative spin densities show a slightly non-linear dependency with respect to the relative dose values. Therefore, a 3rd order polynomial function was fitted to the data. In the following this polynomial model is applied to the EPRI experiments to convert relative spin density distributions to relative dose distributions.

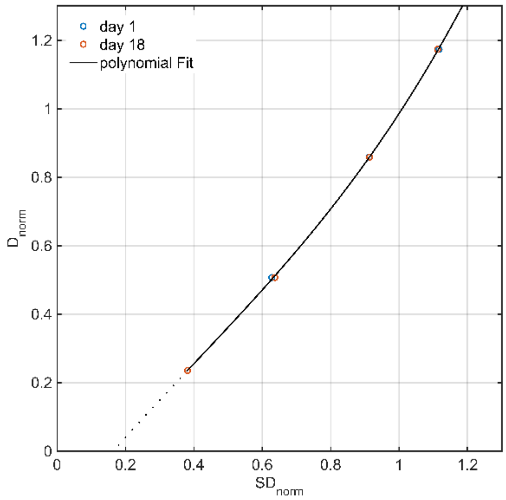

Figure 5: Dependency of relative spin densities (SD_{norm}) derived from 1D-EPRI measurements on the dose (D_{norm}) normalized to an irradiation of 600 Gy. The results for day 1 and day 18 post irradiation are shown. The SD-dose dependency is modelled by a 3rd order polynomial fit.

3.2 EPRI and MC simulation results

The dose distributions resulting from the EPRI measurement are shown in Figure 6 (left side). For comparison the corresponding MC simulation results are shown on the right side. The measured results are presented in the 'imaging coordinate system', whereas the simulation results are displayed in the 'irradiation coordinate system'. In this graphic representations the radiation beam enters the quartz sample from above, i.e. the beam direction points along the –y or –z-direction, respectively. The magnetic field during irradiation is to be imagined pointing along the +x or –y-direction, respectively.

By analysing the simulated raw data, it was noticed that the mean dose to the quartz tube did not differ by more than 1.2 % between the three simulations. To compare the relative dose distributions, the dose colormaps were normalized to the corresponding mean dose value.

Likewise, the reconstructed spin density values were normalized to the mean intensity value inside the quartz and then the relative spin density distributions were converted to dose distributions using the previously derived polynomial function. As in the case of the MC simulations, the resulting measured dose distributions are thus normalized to the mean doses across the quartz samples. The polynomial model is based on 1D-EPRI measurements in the dose range 141 Gy – 704 Gy and may not be applied at lower doses. Hence, dose values below 25 % of the mean dose (600 Gy) are omitted by the color scales in Figure 6.

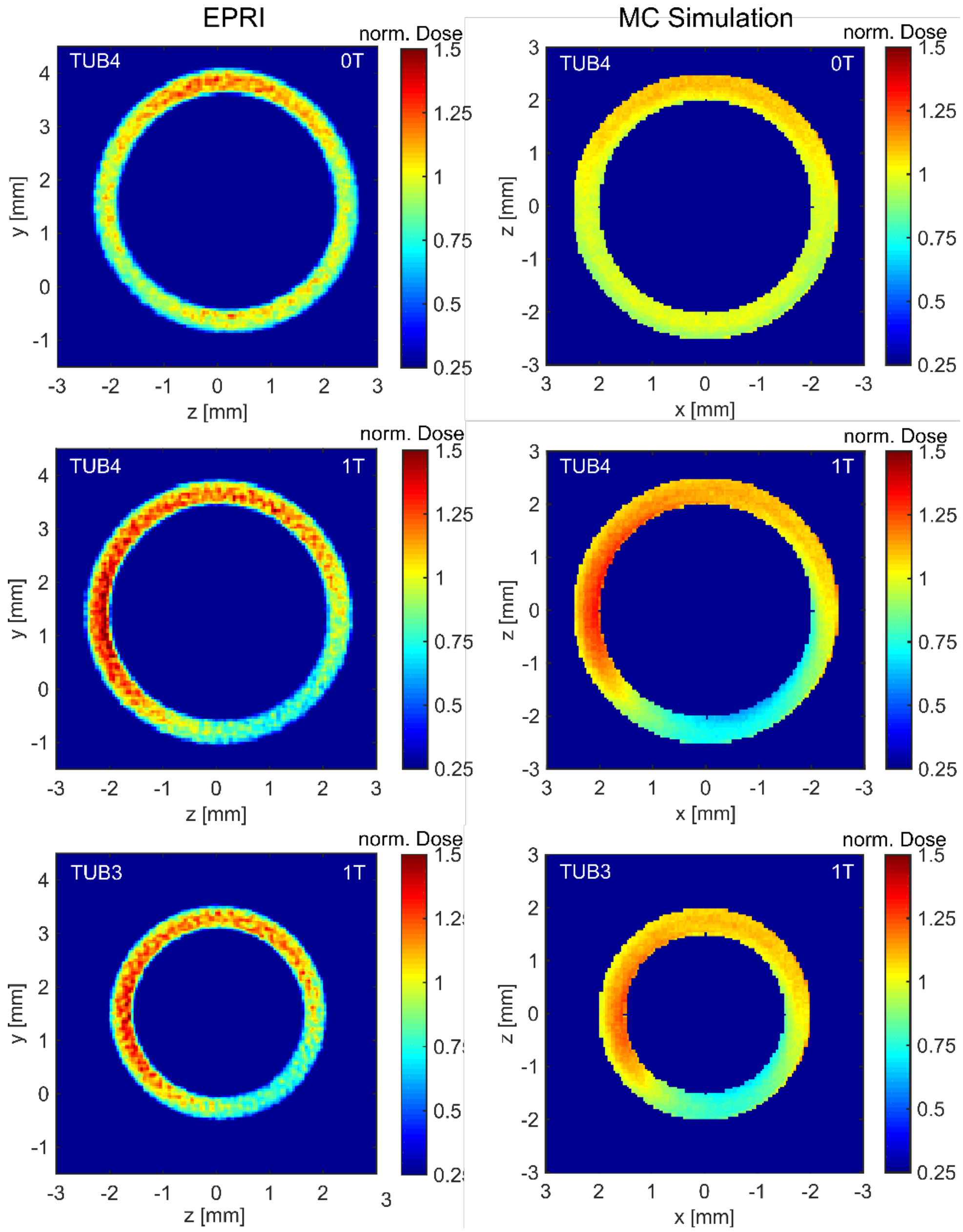

Figure 6: Comparison of reconstructed 2D-EPRI images presented in the 'imaging coordinate system' (left) and corresponding MC simulation results (right) in the 'irradiation coordinate system' for the sample TUB4 irradiated in no external magnetic field (top), TUB4 (middle) and TUB3 (bottom) irradiated in the presence of a 1.0 T magnetic field. The reconstructed relative spin densities were converted to relative dose values as described in the text. The dose values of the MC-Simulation are normalized to the mean dose in the quartz tube.

By comparing the EPRI results for the TUB4 samples one can clearly observe magnetic field induced perturbations of the dose distribution inside the quartz. The dose homogeneity is substantially decreased. This magnetic field induced asymmetry is also seen in the MC simulation results. The measured dose distribution obtained for the TUB3 sample shows similar dose enhancements and reductions within the sample. As an artefact of image reconstruction the edges of the quartz tube wall are blurred. This is mainly due to the inherent high frequency filtering applied during regularized deconvolution.

For better comparison and to further examine the perturbation of the dose distribution over the quartz tubes, a polar coordinate transformation was applied to the 2D-dose distribution obtained in the presence of the 1 T magnetic field. The dose values were radially averaged across the quartz tube wall and the standard errors of the mean values were determined. The polar angle was defined in relation to the y- ('imaging coordinate system') or z-axis ('irradiation coordinate system'). In the graphic representations given in Figure 6 the polar angle increases clockwise. The resulting circular dose distributions are shown in Figure 7. A shift of +10 degrees had to be applied to the EPRI results to correct a rotational setup error.

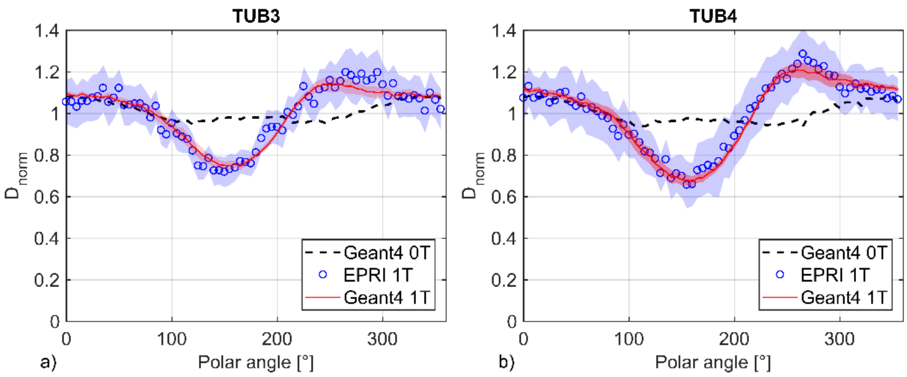

Figure 7: Circular dose distributions over the quartz sample tubes TUB3 (a) and TUB4 (b) after polar coordinate transformation and radial averaging as described in the text. Measured and simulated dose distributions are shown for the case of irradiation in the presence of a 1 T external magnetic field. For comparison purposes, the corresponding simulated dose distribution obtained for zero magnetic field is displayed. The displayed confidence bounds are the standard errors of the mean dose values resulting from radial averaging.

For the samples irradiated in the magnetic field of 1 Tesla dose enhancements of up to 20% (TUB3) and 28% (TUB4) with respect to the mean dose were measured. The polar angle of maximum dose deposition for TUB3 and TUB4 lies between 250° and 280°. On the other hand, substantial dose reduction of up to -28% (TUB3) and -35% (TUB4) for a polar angle between 140°-160° arise. The measured dose distributions are in good agreement with the MC simulation results as the displayed confidence bounds overlap. A gamma analysis according to Low et al. [20] was performed to quantitatively compare the measured and simulated circular dose distributions. For a 3%/10° local gamma criterion more than 93% of the data points obtained via EPRI (Fig. 7) yield a gamma value below 1 when compared to the simulated data.

4. Discussion

So far, only few studies have shown the applicability of EPRI in the field of medical radiation science. Relative dose distributions in human bone samples as well as in hydroxyapatite phantoms could be reconstructed using X-Band Continuous Wave (CW) EPRI [21]. The samples were irradiated in the vicinity of gamma radiation sources typically used in brachytherapy applications (i.e. Iodine-125, Iridium-192). Vanea et al. [22] used L-Band CW-EPRI and solid lithium formate to depict the steep dose gradients around brachytherapy sources. Kolbun et al. [23] measured the dose distribution in lithium formate and ammonium formate when irradiated in the vicinity of an Ir-192 source.

In this work, spin-echo detected EPRI was applied for the first time to determine relative dose distributions around small, cylindrical air cavities (I.D. of 3 or 4mm) in the presence or absence of a transverse, homogeneous magnetic field of approximately 1.0 Tesla – a highly topical issue regarding the introduction of MRgRT in the clinic.

The measurements are based on the EPR absorption spectrum of the well-known, radiation induced E' defects in fused quartz [24]. This is the main class of EPR-active defects in the basic Si-O4 tetrahedra structure originating from an oxygen vacancy. It is described by an unpaired electron in a non-bonding sp3 hybrid oribtal on a silicon [25,26,27]. Impurities in the quartz may lead to additional EPR active defects generated upon irradiation [28]. Besides, two variants of oxygen associated trapped hole centers (OHC) could be identified in irradiated fused quartz [29]. Their relative prevalence depends on the OH content of the specific glass. Moreover, a peroxy radical was found in irradiated fused quartz [30]. Hence, the EPR characteristics of irradiation induced EPR-active defects in quartz may vary depending on the impurity content and manufacturing process [14,25,31]. Therefore, the dose-dependence of crucial EPR characteristics (temporal stability, spectral shape and spin relaxation times) need to be examined for each specific type of quartz glass prior to the measurement of dose distributions via spin-echo detected EPRI. For the purpose of the experimental procedure described here, no relevant dose-dependencies of these EPR characteristics were observed for the fused quartz samples used in this work.

Pulsed EPR was applied since the known long spin relaxation times of the irradiation induced defects in fused quartz samples make it difficult to obtain unsaturated CW-EPR spectra free of passage effects [32]. Moreover, spin-echo detected EPRI has been already demonstrated for irradiated quartz samples by Eaton and Eaton [33].

Although a linear signal-dose response in the kGy dose range is expected from the literature [34,35], a monotoneous, slightly non-linear dose dependence of the reconstructed spin density was observed (Figure 5) for the dose range investigated in this work. The 1D-EPRI experimental procedure showed a high degree of reproducibility since the differences between independent measurements (day 1 and day 18) are within uncertainties. The SD-dose dependency below 141 Gy remains unclear. The polynomial model predicts an unreasonable non-zero signal intensity for zero dose. It is known from the literature that different types of E' defects may be generated upon irradiation [34,36]. It was also reported that for the dose range investigated in this work defects are generated rather from precursors [35] than from direct matrix activation. The slight non-linear SD-dose dependency as well as the non-zero signal intensity predicted for zero dose is presumably resulting from an underlying irradiation induced defect species that saturates at doses below 141 Gy.

The data postprocessing performed in this work included the conversion of the measured relative spin density distributions to relative dose distributions by applying the experimentally derived polynomial model to the measured image values. To check the validity of the entire method, the postprocessed, experimental results were compared to MC simulation results.

MC simulations are a reliable tool to calculate dose distributions in radiotherapy. Geant4 [16] is a simulation toolkit capable of simulating particle transport through matter in the presence of external magnetic fields. It was validated for medical physics applications [37,38] and has been used in numerous studies to examine magnetic field induced perturbations on dose distributions in the context of MRgRT (e.g. [8,39,40,41]).

The experimental results of this work clearly depict the substantial influence of the external magnetic field on the dose distribution within the sample material surrounding the air cavity. The experimentally derived circular dose distributions are quantitatively in good agreement (passrate > 93% for 3%/10° gamma criterion) with the corresponding MC simulation results. These findings support the applicability of the experimental procedure. The circular dose distributions show dose enhancements of up to 20% (TUB3) and 28% (TUB4) with respect to the mean dose at a polar angle between 250° and 280°. On the other hand, substantial dose reduction of up to -28% (TUB3) and -35% (TUB4) at a polar angle between 140°-160° arise. Thus, this work provides experimental evidence that for cylindrical air cavities with a diameter of 3-4 mm the dose perturbations induced by the ERE are not fully compensated by applying parallel opposed beam configurations. This effect was already shown for an air tube with a diameter of 2 cm by Raaijmakers et al. [8] using MC simulations.

For an additional plausibility check one can estimate the radius of curvature in vacuum for the trajectories of electrons released during irradiation. According to Raaijmakers et al. [8], reasonable assumptions for calculating the mean electron energy are that the mean photon energy is given by one third of the accelerator voltage and that the mean kinetic energy of the electron spectrum is approximately one quarter of the average photon energy. For a 6 MV photon beam the mean electron energy is thus estimated to about 0.5 MeV. Given a magnetic field strength of 1.0 Tesla the radius of curvature for an electron with a kinetic energy of 0.5 MeV is approximately 2.9 mm. The diameters of the air-filled cavities studied in this work are about in the same order (3-4 mm). Therefore, one had to expect perturbations of dose distributions in the quartz sample tube surrounding the air cavity due to the ERE: Electrons entering the air cavity start to spiral clockwise (with respect to the graphic representations given in Figure 6) due to the Lorentz force.

Recent studies have shown the applicability of EBT3 radiochromic film [42] as well as 3D detectors such as radiochromic plastic, radiochromic gel and polymer gel [43,44] for the

purpose of relative dosimetry in the presence of strong magnetic fields. More recently, Presage® radiochromic plastic was tested for dosimetry at phantom-air interfaces [45,46] and showed good agreement with Monte Carlo (MC) radiation transport simulations.
The results of this work show the feasibility of spin-echo detected EPRI to determine magnetic field induced perturbations of dose distributions around small, cylindrical air cavities (diameter 3 - 4 mm). High spatial resolutions (below 100 µm) can be achieved when fused quartz is used as a probe material, yet high doses (600 Gy) are needed to obtain a sufficient signal-to-noise ratio within a measuring time of 24 hours.
Future research may address other EPR imaging techniques like Rapid Scan EPR Imaging [32,47] to further enhance the sensitivity per unit time of EPRI and consequently to reduce the irradiation doses and measurement time needed. Besides, EPRI can also be performed in three spatial dimensions and may thus serve as a future volumetric dosimetry tool.
Primarily due to its density of about 2.2 g/cm^3 fused quartz is lacking water equivalence. In combination with an increased detection sensitivity EPRI can potentially be applied to porouse quartz samples with reduced bulk density. Furthermore, the presented EPRI method is not restricted to fused quartz samples but applicable to possible sample materials meeting the call for water equivalence and simultaneously exhibiting appropriate characteristics for EPRI.

5. Conclusion

In this work, spin-echo detected EPRI was applied for the first time to determine relative dose distributions around small, cylindrical air cavities (I.D. of 3 or 4mm) in the presence or absence of a transverse, homogeneous magnetic field of approximately 1.0 Tesla.
The results provide experimental evidence for the electron return effect (ERE) occuring already for air cavities of milimeter size.
The experimentally derived circular dose distributions are quantitatively in good agreement (passrate > 93% for 3%/10° gamma criterion) with the corresponding MC simulation results. These findings confirm the feasibility of the experimental procedure.
EPRI may thus play a future role for the investigation of dose distributions at tissue-air interfaces and may serve as an experimental dosimetry tool to validate clinial dose calculation algorithms that are applied during therapy planning in the context of MRgRT.
Although high doses (600 Gy) are needed to obtain a sufficient signal-to-noise ratio within a measuring time of 24 hours when fused quartz is used as sample material, the sensitivity per unit time may be increased in the future by applying Rapid Scan EPRI.

Acknowledgements

All authors and co-authors disclose any potential conflict of interest. The authors gratefully acknowledge the help of Daniel Frei from Inselspital in Bern regarding the implementation of the phase-space file into the Geant4 MC simulation code. Edmond Sterpin was partially supported by Accuray for the simulation of the TomoTherapy machine.

References

[1] Dempsey J F, Benoit D, Fitzsimmons J R, Haghighat A, Li J G, Low D A, Sjoden G E 2005 A Device for Realtime 3D Image-Guided IMRT *International Journal of Radiation Oncology * Biology * Physics* **63** 202

[2] Raaymakers B W *et al*. 2009 Integrating a 1.5 T MRI scanner with a 6 MV accelerator: proof of concept *Phys. Med. Biol.* **54** 229

[3] Fallone B G *et al*. 2009 First MR images obtained during megavoltage photon irradiation from a prototype integrated linac-MR system *Medical Physics* **36** 2084–2088

[4] Oborn B M, Kolling S, Metcalfe P E, Crozier S, Litzenberg D W, and Keall P J 2014 Electron contamination modelling and reduction in a 1 T open bore inline MRI-linac system *Medical Physics* **41** 051708

[5] Raaymakers B W *et al.* 2017 First patients treated with a 1.5 T MRI-Linac: clinical proof of concept of a high-precision, high-field MRI guided radiotherapy treatment *Phys. Med. Biol.* **62** 23

[6] Mutic S and Dempsey J F 2014 The ViewRay System: Magnetic Resonance–Guided and Controlled Radiotherapy *Seminars in Radiation Oncology* **24** 196–199

[7] Raaymakers B W, Raaijmakers A J E, Kotte A N T J, Jette D and Lagendijk J J W 2004 Integrating a MRI scanner with a 6 MV radiotherapy accelerator: dose deposition in a transverse magnetic field *Phys. Med. Biol.* **49** 4109

[8] Raaijmakers A J E, Raaymakers B W and Lagendijk J J W 2005 Integrating a MRI scanner with a 6 MV radiotherapy accelerator: dose increase at tissue–air interfaces in a lateral magnetic field due to returning electrons *Phys. Med. Biol.* **50** 1363

[9] Richter S, Pojtinger S, Mönnich D, Dohm O S and Thorwarth D 2017 Influence of a transverse magnetic field on the dose deposited by a 6 MV linear accelerator *Current Directions in Biomedical Engineering* **3** 281

[10]Rubinstein A E, Gay S, Peterson C B, Kingsley C V, Tailor R C, Pollard-Larkin J M, Melancon A D, Followill D S and Court L E 2018 Radiation-induced lung toxicity in mice irradiated in a strong magnetic field PLOS ONE **13** e0205803

[11]Ahmad S B, Sarfehnia A, Paudel M R, Kim A, Hissoiny S, Sahgal A and Keller B 2016 Evaluation of a commercial MRI Linac based Monte Carlo dose calculation algorithm with geant 4 Medical Physics **43** 894–907

[12]Lund A and Shiotani M 2014 Applications of EPR in Radiation Research (Cham: Springer International Publishing)

[13]Eaton G R and Eaton S S 1995 Introduction to EPR imaging using magnetic-field gradients Concepts Magn. Reson. **7** 49–67

[14]León M, Martín P, Ibarra A and Hodgson E R 2009 Gamma irradiation induced defects in different types of fused silica Journal of Nuclear Materials **386–388** 1034–7

[15]Ziaie F, Mohammadzadeh A and Modarresi M 2009 Stability study of free radicals in 10 MeV electron beam irradiated quartz as an EPR dosimetry method Nukleonika **54** 251–4

[16]Agostinelli S et al. 2003 Geant4 - a simulation toolkit Nuclear Instruments and Methods in Physics Research Section A: Accelerators, Spectrometers, Detectors and Associated Equipment, **506** 3 250

[17]Spitzbarth M and Drescher M 2015 Simultaneous iterative reconstruction technique software for spectral–spatial EPR imaging Journal of Magnetic Resonance **257** 79–88

[18]Lee J, Lee J, Ryu D, Lee H and Ye S-J 2018 Fano cavity test for electron Monte Carlo transport algorithms in magnetic fields: comparison between EGSnrc, PENELOPE, MCNP6 and Geant4 Phys. Med. Biol. **63** 195013

[19]Sterpin E, Tomsej M, Cravens B, Salvat F, Ruchala K, Olivera G H and Vynckier S 2007 Monte Carlo simulation of the Tomotherapy treatment unit in the static mode using MC HAMMER, a Monte Carlo tool dedicated to Tomotherapy J. Phys.: Conf. Ser. **74** 021019

Cite also: [1] E. Sterpin et al., Phys. Med. Biol. 53 (2008) 2161–2180.

[20]Low D A, Harms W B, Mutic S and Purdy J A 1998 A technique for the quantitative evaluation of dose distributions Medical Physics **25** 656–61

[21]Levêque P, Godechal Q, Bol A, Trompier F and Gallez B 2009 X-band EPR imaging as a tool for gradient dose reconstruction in irradiated bones Med. Phys. **36** 4223–9

[22]Vanea E S, Levêque P, Abboud F, Bol A, Denis J M, Kolbun N, Vynckier S and Gallez B 2009 Evaluation of the dose distribution gradient in the close vicinity of brachytherapy seeds using electron paramagnetic resonance imaging Magn. Reson. Med. **61** 1225–31

[23]Kolbun N, Adolfsson E, Gustafsson H and Lund E 2014 High-resolution mapping of 1D and 2D dose distributions using X-band electron paramagnetic resonance imaging Radiat. Prot. Dosim. **159** 182–7

[24]Agnello S, Boscaino R, Cannas M and Gelardi F M 2001 Instantaneous diffusion effect on spin-echo decay: Experimental investigation by spectral selective excitation Phys. Rev. B **64** 174423

[25]Weeks R A 1956 Paramagnetic Resonance of Lattice Defects in Irradiated Quartz Journal of Applied Physics **27** 1376–81

[26]Silsbee R H 1961 Electron Spin Resonance in Neutron-Irradiated Quartz Journal of Applied Physics **32** 1459–62

[27]Yip K L and Fowler W B 1975 Electronic structure of E' centers in SiO2 Phys. Rev. B **11** 2327–38

[28]Feigl F J and Anderson J H 1970 Defects in crystalline quartz: Electron paramagnetic resonance of E' vacancy centers associated with germanium impurities Journal of Physics and Chemistry of Solids **31** 575–96

[29]Stapelbroek M, Griscom D L, Friebele E J and Sigel G H 1979 Oxygen-associated trapped-hole centers in high-purity fused silicas Journal of Non-Crystalline Solids **32** 313–26

[30]Friebele E J, Griscom D L, Stapelbroek M and Weeks R A 1979 Fundamental Defect Centers in Glass: The Peroxy Radical in Irradiated, High-Purity, Fused Silica Phys. Rev. Lett. **42** 1346–9

[31]Galeener F L, Kerwin D B, Miller A J and Mikkelsen J C 1993 X-ray creation and activation of electron spin resonance in vitreous silica Phys. Rev. B **47** 7760–79

[32]Mitchell D G, Quine R W, Tseitlin M, Meyer V, Eaton S S and Eaton G R 2011 Comparison of Continuous Wave, Spin Echo, and Rapid Scan EPR of Irradiated Fused Quartz Radiat Meas **46** 993–6

[33]Eaton G R and Eaton S S 1986 Electron spin-echo-detected EPR imaging Journal of Magnetic Resonance (1969) **67** 73–7

[34]Agnello S, Boscaino R, Buscarino G, Cannas M and Gelardi F M 2002 Structural relaxation of E' centers in amorphous silica Phys. Rev. B **66** 113201

[35]Mashkov V A, Austin W R, Zhang L and Leisure R G 1996 Fundamental Role of Creation and Activation in Radiation-Induced Defect Production in High-Purity Amorphous SiO2 Phys. Rev. Lett. **76** 2926–9

[36]Griscom D L 1984 Characterization of three E'-center variants in X- and γ-irradiated high purity a-SiO2 Nuclear Instruments and Methods in Physics Research Section B: Beam Interactions with Materials and Atoms **1** 481–8

[37]Carrier J-F, Archambault L, Beaulieu L and Roy R 2004 Validation of GEANT4, an object-oriented Monte Carlo toolkit, for simulations in medical physics Medical Physics **31** 484–92

[38]Raaijmakers A J E, Raaymakers B W and Lagendijk J J W 2007 Experimental verification of magnetic field dose effects for the MRI-accelerator Phys. Med. Biol. **52** 4283

[39]Mahdavi S R, Esmaeeli A D, Pouladian M, Monfared A S, Sardari D and Bagheri S 2015 Breast dosimetry in transverse and longitudinal field MRI-Linac radiotherapy systems Medical Physics **42** 925–36

[40]Oborn B M, Metcalfe P E, Butson M J and Rosenfeld A B 2009 High resolution entry and exit Monte Carlo dose calculations from a linear accelerator 6 MV beam under the influence of transverse magnetic fields Medical Physics **36** 3549–59

[41]Oborn B M, Metcalfe P E, Butson M J and Rosenfeld A B 2010 Monte Carlo characterization of skin doses in 6 MV transverse field MRI-linac systems: Effect of field size, surface orientation, magnetic field strength, and exit bolus Medical Physics **37** 5208–17

[42]Delfs B, Schoenfeld A A, Poppinga D, Kapsch R-P, Jiang P, Harder D, Poppe B and Looe H K 2017 Magnetic fields are causing small, but significant changes of the radiochromic EBT3 film response to 6 MV photons *Phys. Med. Biol.* **63** 035028

[43]Lee H J, Roed Y, Venkataraman S, Carroll M and Ibbott G S 2017 Investigation of magnetic field effects on the dose–response of 3D dosimeters for magnetic resonance – image guided radiation therapy applications *Radiotherapy and Oncology* **125** 426-432

[44]Lee H J, Kadbi M, Bosco G and Ibbott G S 2018 Real-time volumetric relative dosimetry for magnetic resonance – image-guided radiation therapy (MR-IGRT) *Phys. Med. Biol.* **63** 045021

[45] Costa F, Doran S J, Hanson I M, Nill S, Billas I, Shipley D R, Duane S, Adamovics J and Oelfke U 2018 Investigating the effect of a magnetic field on dose distributions at phantom-air interfaces using PRESAGE® 3D dosimeter and Monte Carlo simulations *Phys. Med. Biol.* **63** 05NT01

[46]Lee H J, Choi G W, Alqathami M, Kadbi M and Ibbott G 2017 Using 3D dosimetry to quantify the Electron Return Effect (ERE) for MR-image-guided radiation therapy (MR-IGRT) applications *J. Phys.: Conf. Ser.* **847** 012057

[47]Eaton S S, Shi Y, Woodcock L, Buchanan L A, McPeak J, Quine R W, Rinard G A, Epel B, Halpern H J and Eaton G R 2017 Rapid-scan EPR imaging *Journal of Magnetic Resonance* **280** 140–8